Quantum energy gap law of outer-sphere electron transfer reactions: A molecular dynamics study on aqueous solution

Koji Ando

Citation: The Journal of Chemical Physics **106**, 116 (1997); doi: 10.1063/1.473037
View online: http://dx.doi.org/10.1063/1.473037
View Table of Contents: http://scitation.aip.org/content/aip/journal/jcp/106/1?ver=pdfcov
Published by the AIP Publishing

Quantum energy gap law of outer-sphere electron transfer reactions: A molecular dynamics study on aqueous solution

Koji Ando
The Institute of Physical and Chemical Research (RIKEN), Wako, Saitama 351-01, Japan and Institute of Materials Science, University of Tsukuba, Tsukuba, Ibaraki 305, Japan[a)]

(Received 22 July 1996; accepted 26 September 1996)

The quantum energy gap law for electron transfer (ET) reactions in water is examined. Molecular dynamics (MD) simulation analysis is carried out to obtain the solvent reorganization energies, time correlation functions (TCF), spectral density functions, and quantum rate constants. Their dependence on the reaction free energy and on the donor–acceptor distance is explored along with the solvent isotope effects. Properties of the imaginary-time saddle-point for the TCF expression of the ET rate formula are also examined. The high-frequency intramolecular vibrational modes of the solvent water are found to present marked quantum effects on the ET rate, while their contribution to the static reorganization energy is small (less than 6%). The energy gap dependence of the quantum activation free energy is shown to become nearly independent of the donor–acceptor distance when renormalized by the reorganization energy. Approximations to compute quantum rate constants from MD simulation data are briefly discussed in light of of the present results. © *1997 American Institute of Physics.* [S0021-9606(97)51501-7]

I. INTRODUCTION

Electron transfer (ET) reactions are among central elementary processes in chemistry and biochemistry.[1–4] Above all, ET in water is of particular interest in the following aspects besides the prevalent importance of water: (1) Because of the high polarity of water, the solvent polarization couples to the ET process strongly. (2) Dynamics of the polarization reorganization of water are primarily described by the librational motions involving displacements of the light hydrogen atoms, which may thus present notable quantum effects. The subject of this paper is to elucidate this solvent nuclear quantum aspect of ET reactions in water.

We employ the harmonic bath model coupled to a two-state system. Thus it is essential to evaluate the spectral density functions of the bath modes,[5] which we achieve with a realistic molecular dynamics (MD) simulation analysis.[6–8] Our focus is on the dependence of the ET rate on the reaction exothermicity (the energy gap law),[9–12] and on the quantum solvent nuclear effects including the solvent isotope effect. The importance of the intramolecular vibrational motions of the solvent water is stressed, which are shown to present marked quantum effects despite that they do not contribute much to the static energetics (especially the solvent reorganization energy) and have been neglected in many of the previous simulation studies on aqueous ET.

The role of the high-frequency vibrational modes exploited here is conceptually rather different from that considered in previous works. The latter was primarily for the solute intramolecular modes involving large structural changes coupled to ET, i.e., the ''inner-sphere'' reorganizations. In contrast, it is shown here that the stretching and bending modes of the solvent water comes into prominence when the quantum aspects of ET rates are considered, while their contribution in the static reorganization energy is quantitatively small.

The solvent reorganization energy is a key quantity determining the ET rate and mechanism. Figure 1 displays a schematic picture of the free energy diagram of ET reactions. The abscissa denotes a solvent coordinate measuring the collective solvent polarization (predominantly orientational) coupled to ET. A precise definition of the solvent coordinate employed in this work is given in Sec. III. Marcus derived the following formula for the activation free energy ΔF^* of ET reactions:[4]

$$\Delta F^* = (\Delta F^0 + \lambda)^2/4\lambda, \tag{1.1}$$

which predicts that the log-plot of the ET rate as a function of the reaction free energy ΔF^0 shows an inverted parabola with the maximum at $\Delta F^0 = -\lambda$, i.e., the reaction exothermicity equal to the solvent reorganization energy λ. This is a consequence of the linear response assumption and the resulting parabolic free energy curves along the solvent polarization coordinate. Namely, the actual coordinates of each solvent molecule are not necessarily described by harmonic oscillators, but given that the collective solvent polarization follows the linear response then the classical activation free energy is expressed by Eq. (1.1).

An equivalent[13] of Eq. (1.1) was also derived by Kubo and Toyozawa[14] as the high-temperature limit of the golden-rule rate formula for nonradiative electronic transitions coupled to phonons. Warshel and co-workers[6] developed a simulation method to apply the time correlation function (TCF) formula[14,15] for solution phase ET problems by representing the solvent polarization in terms of a collection of effective harmonic oscillators obtained from the Fourier components of the MD trajectories. This method was further examined by Bader *et al.*[7] who showed that the ''semiclassical'' approximation (here, this term specifies a neglect of

[a)]Present and permanent address.

 0021-9606/97/106(1)/116/11/$10.00

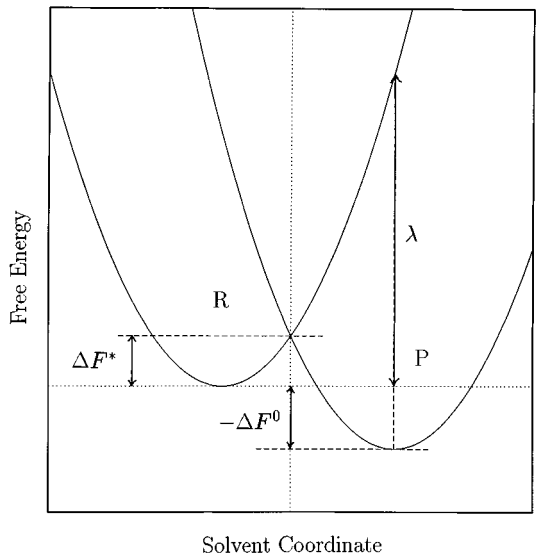

FIG. 1. Schematic illustration of the free energy curves of electron transfer reactions in the solvent polarization coordinate. The labels *R* and *P* denote the initial reactant and the final product states, respectively.

the commutator $[H_i, H_f]$, where H_i and H_f denote the Hamiltonians of the initial and final electronic states, respectively[11,16]) to the TCF formula is unnecessary, and that the ET rate constant is usefully evaluated by the method of steepest-descents.[2,11] It is noted that the ET system studied by Bader *et al.* is a symmetric ferrous-ferric electron exchange reaction with $\Delta F^0=0$ for which the imaginary-time saddle-point is automatically given by the symmetry.

There could be at least two directions to proceed upon these achievements. The first would relax the harmonic bath approximation and compute the quantum activation free energy using, e.g., the path-integral quantum Monte Carlo (PIQMC) technique.[7,17,18] The second direction, which we pursue here, extends the saddle-point method for asymmetric ($\Delta F^0 \neq 0$) systems. The linear response assumption with the Gaussian bath model seems quite accurate for ET in water,[6,7,19–21] primarily due to the long-range nature of the electrostatic interaction (and the central-limit theorem for the coupled many degrees of freedom). Although there exists a previous study[11] on the energy gap law that applies the saddle-point method to a hypothetical system with small degrees of freedom, to our knowledge, there is no extensive study along this line based on realistic MD simulations with an account on the critical roles of the intramolecular vibrations of water.

In this work, we carry out a MD simulation analysis on a model charge-separation ET,

$$D(aq)+A(aq) \rightleftharpoons D^+(aq)+A^-(aq), \tag{1.2}$$

in a flexible model of water. The donor and acceptor molecules are modeled each by a spherical cavity with a central point charge and a short-range Lennard-Jones core. We previously reported[22] a study on a specific molecular system (photoinduced ET between N,N-dimethylaniline and anthracene in acetonitrile solution) in which *ab initio* molecular orbital calculations were combined with MD simulations. It would be also useful to simplify the solute model, which allows us to take the energy gap ΔF^0 as a variable parameter rather than a system specific quantity, and to focus on the solvent originated properties.

It is noted that meaningful comparison with experiments is achieved by extensive modeling studies on a series of specific systems, for which various factors such as the electronic coupling, molecular shape and size, and the interaction energetics do differ from each other even for a collection of related systems. Above all, *ab initio* evaluation of the electronic coupling and its dependence on the solvent configuration, along with the solution phase energetics and dynamics, is one of the most important open questions.[22,23] While our studies along these lines are under way, we report the present work to illuminate the solvent properties.

The organization of this paper is as follows. The next section summarizes the simulation methods. Section III discusses the results of the simulation analysis, which include the solvent reorganization energies, the time correlation functions, the relaxation time constants, the spectral density functions, and the quantum rate constants. Their dependence on the donor–acceptor distance and on the energy gap are investigated along with the solvent isotope effects. Some properties of the imaginary-time saddle-point of the ET rate expression are also examined. The importance of the high-frequency intramolecular vibrations of the solvent water is quantified by comparing with a rigid water model and by analyzing the spectral density functions. Finally, approximations to compute quantum rate constants from MD simulations are briefly discussed in light of the ET energy gap law with the present simulation results. The final section concludes.

II. SIMULATION METHODS

The MD simulations are performed for a system that consists of an electron donor–acceptor pair surrounded by 500 solvent water molecules in a cubic simulation box with a periodic boundary condition.[24] The donor and acceptor are represented each by a spherical cavity with a central point charge and a 12-6 Lennard-Jones core. A flexible TIP3P model[25] of water with the intramolecular potential function developed by Dang and Pettitt[26] is employed. The intermolecular potentials are represented by a form

$$V_{\mathrm{int}}=\sum_{I>J}\left[\frac{q_I q_J}{r_{IJ}}+4\epsilon_{IJ}\left\{\left(\frac{\sigma_{IJ}}{r_{IJ}}\right)^{12}-\left(\frac{\sigma_{IJ}}{r_{IJ}}\right)^{6}\right\}\right], \tag{2.1}$$

in which r_{IJ} denotes the distance between the atom positions I and J. The potential parameters are; $q_{\mathrm{O}}=-0.834e$, $q_{\mathrm{H}}=0.417e$, $\epsilon_{\mathrm{OO}}=0.152$, $\epsilon_{\mathrm{HH}}=0$, $\epsilon_{dd}=0.5$, $\epsilon_{aa}=0.5$, $\sigma_{\mathrm{OO}}=3.15$, $\sigma_{\mathrm{HH}}=0$, $\sigma_{dd}=7.0$, $\sigma_{aa}=7.0$ (ϵ and σ are in kcal/mol and in Å), where the subscripts d and a denote the donor and acceptor, respectively. The conventional combining rule, such as $\epsilon_{IJ}=\sqrt{\epsilon_{II}\epsilon_{JJ}}$, is employed. The parameters for the donor–acceptor pair are chosen rather arbitrarily, but refer to those for organic molecules often used in experimental ET studies. The charge parameters for the solute are $q_d=q_a=0$

for the initial reactant state and $q_d=+1$, $q_a=-1$ for the product state, representing the charge-separation ET. The mass density is set to be 0.982 g/cm^3 which is from a constant pressure Monte Carlo study[25] on the rigid TIP3P water at 25 °C, 1 atm. The dimension of the simulation box is then 25.06 Å. The mass of the donor and acceptor spheres are put arbitrarily to be those for $C_8H_{11}N$ and $C_{14}H_{10}$, respectively.[22] In all the simulations reported here, the donor–acceptor distance is fixed by treating the pair as a diatomic. The interaction potentials are smoothly cut-off in the region $0.45L<r_{ij}<0.5L$ (L=simulation box length) with a fifth-order polynomial function.[20]

Integration of the equations of motion is performed by the four-value Gear predictor–corrector method[27] which is initiated by the fourth-order Runge–Kutta method.[28] The Gear method is not self-starting since it utilizes the third and fourth time derivatives of the positions. Thus the first step of the trajectory is initiated by the Runge–Kutta method with the time step of $\Delta t/4$, and then the trajectory is numerically differentiated to produce the higher derivatives. The time step used is $\Delta t=0.1$ fs, which gives good total energy conservation; the average rms (root-mean-square) deviation of the total energy was 0.03 ± 0.02 and 0.005 ± 0.0002 kcal/mol for H_2O and D_2O solvents, respectively. Another criterion for the trajectory accuracy is the ratio[29]

$$\Delta E(\mathrm{rms})/\Delta KE(\mathrm{rms}) \tag{2.2}$$

between the rms fluctuations of the total energy $\Delta E(\mathrm{rms})$ and the total kinetic energy $\Delta KE(\mathrm{rms})$, for which we obtained 0.0014 ± 0.0001 and 0.00022 ± 0.00001 for H_2O and D_2O systems, respectively. Equilibrium MD calculations were carried out for 5×10^5 steps (=50 ps) after careful cooling and equilibration runs.[30] No temperature controlling algorithm was used in the production runs. The resultant kinetic temperatures were found to be in a range 298–306 K. This dispersion of ~8 K is energetically irrelevant for the present study. The rms fluctuation of the kinetic temperature in the microcanonical system was typically 6 K.

A comparison with the rigid TIP3P water model is also made in Secs. III A and III E to highlight the solvent intramolecular vibrational effects. Quarternion parameters are used to describe the rotational motion of the rigid water. The five-values Gear algorithm is employed for the first-order equations of motion. The time step used is $\Delta t=0.5$ fs. The equilibrium production runs were performed for 50 ps. The rms deviation of the total energy was 0.197 ± 0.002 kcal/mol, and the other criterion of Eq. (2.2) was 0.0106 ± 0.0004. The kinetic temperatures were within 296–304 K with the rms fluctuation of ~6 K.

III. RESULTS AND DISCUSSION

A. Solvent reorganization energies

The solvent reorganization energy λ is computed from the equilibrium simulation data by

$$\lambda=(-\langle\Delta V\rangle_i+\langle\Delta V\rangle_f)/2, \tag{3.1}$$

with

TABLE I. Reorganization energy. R and λ are in Å and in eV, respectively.

R	λ (H_2O)	λ (D_2O)	λ (H_2O,rigid)
5	1.842 ± 0.029	1.850 ± 0.030	1.842 ± 0.027
6	⋯	⋯	2.268 ± 0.028
7	2.608 ± 0.042	2.589 ± 0.036	2.615 ± 0.040
8	⋯	⋯	2.995 ± 0.038
9	3.168 ± 0.043	3.203 ± 0.042	3.214 ± 0.038
10	⋯	⋯	3.417 ± 0.039

$$\Delta V\equiv H_i-H_f, \tag{3.2}$$

where $\langle\ldots\rangle_{i,f}$ denotes the equilibrium average in the initial and final states. ΔV could be considered as a microscopic definition of the solvent coordinate as it represents the degree of solvent polarization by measuring the relative potential stability of the two diabatic states i and f at a given solvent configuration.[33] Thus the free energy curves schematized in Fig. 1 can be constructed on a microscopic basis by simulating the thermal probability distribution of this coordinate.[6,20] Equation (3.1) is precise for parabolic free energy curves, the adequacy of which has been demonstrated in many simulation studies of aqueous solutions.[6,7,19–21]

The dependence of λ on the donor–acceptor distance R as well as the solvent isotope effects are summarized in Table I. The reorganization energies for H_2O and D_2O solvents resulted in very close values within the simulation uncertainties.[34] The rigid H_2O model also gave almost the same λ for all R considered. The solvent intramolecular degrees of freedom may couple to ET by changing the net and local dipole of each molecule. However, the simulation results show that their contributions in the static reorganization energy are quantitatively small. Their contributions are clearly seen in the spectral density functions, and are analyzed quantitatively by using the sum relation Eq. (3.10) in Sec. III C.

The R-dependence of λ is one of critical factors determining ET mechanism.[9,12,35] Figure 2 plots λ as a function of $1/R$. The computed λ depends almost linearly on $1/R$, which is in accord with the dielectric continuum prediction,[4,36]

$$\lambda=(\Delta e)^2\left(\frac{1}{\epsilon_\infty}-\frac{1}{\epsilon_0}\right)\left(\frac{1}{2a_a}+\frac{1}{2a_d}-\frac{1}{R}\right). \tag{3.3}$$

Equation (3.3) with the donor and acceptor radii $a_d=a_a=3.5$ Å (see the Lennard-Jones parameters in Sec. II), $\epsilon_\infty=1$, and $\epsilon_0=78.4$ gives the dashed line in Fig. 2. Although the quantitative agreement is poor, the close proximity of the slopes is noted. Another possible definition of the radii may utilize the σ parameters of the solute and the solvent water as, $a_d(=a_a)=\sigma_{Od}\sigma_{dd}/(\sigma_{OO}+\sigma_{dd})=3.24$ Å, which parallelly shifts Eq. (3.3) to give the dash-dotted line. The least-squares fitting to the simulation data gives $a_d=a_a=3.01$ Å (dotted line), which might appear too small for the interaction potential. Such an indefiniteness of the cavity boundary would be inevitable for the dielectric continuum model. However, the agreement of the slopes and the nearly linear dependence on

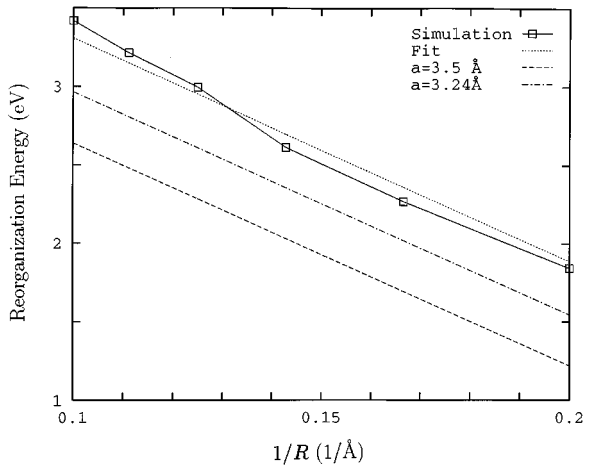

FIG. 2. The solvent reorganization energy as a function of the inverse donor–acceptor distance $1/R$. The simulation data (boxes) shown is for the rigid water model (see Table I). Equation (3.3) with the solute radii $a_d=a_a=3.5$ (dotted), 3.24 (dash-dotted) and 3.01 Å from the least-squares fit (dotted) is included for comparison (see the text).

$1/R$ seems encouraging for the use of the continuum model with some appropriate readjustment of the boundary parameters.

B. Time correlation functions

The classical time correlation functions (TCF) of the solvent coordinate

$$\langle \delta\Delta V(0)\,\delta\Delta V(t)\rangle_{\rm cl}/\langle \delta\Delta V(0)^2\rangle_{\rm cl}, \tag{3.4}$$

where $\delta\Delta V$ denotes the deviation from the thermal average $\delta\Delta V=\Delta V-\langle V\rangle$, are displayed in Fig. 3. The rapid decay within ~25 fs and the subsequent oscillatory behavior with a ~40 fs period are almost the same as those seen in previous simulations[19,20] for unimolecular solutes in rigid water models. The former nearly Gaussian behavior is discussed to originate from inertial motions of the solvent molecules.[37] The latter comes from the libration of water. Although very weak high-frequency components coming from the solvent intramolecular vibrations are seen on the decay curves, the overall profile of the relaxation is determined by the lower-frequency modes that are essentially modeled by rigid water models. As will be discussed in the next subsection, the contributions from the high-frequency vibrations are clearly seen in the spectral density function. Figure 3(a) indicates that the dependence of TCF on R is small. The dependence on the solute state (neutral or ion pair) is also found to be small, similarly to the previous findings.[19,20] The results shown hereafter are primarily for the neutral pair state, except for Fig. 4(b) that compares the spectral density functions of the two states.

Figure 3(b) shows the solvent isotope effects on the TCF. Both the initial rapid decay and the subsequent librational oscillations slow down for D_2O. The period of the D_2O libration is ~55 fs. Figure 3(b) also includes least-squares fit of the TCF to a sum of Gaussian and exponential functions,

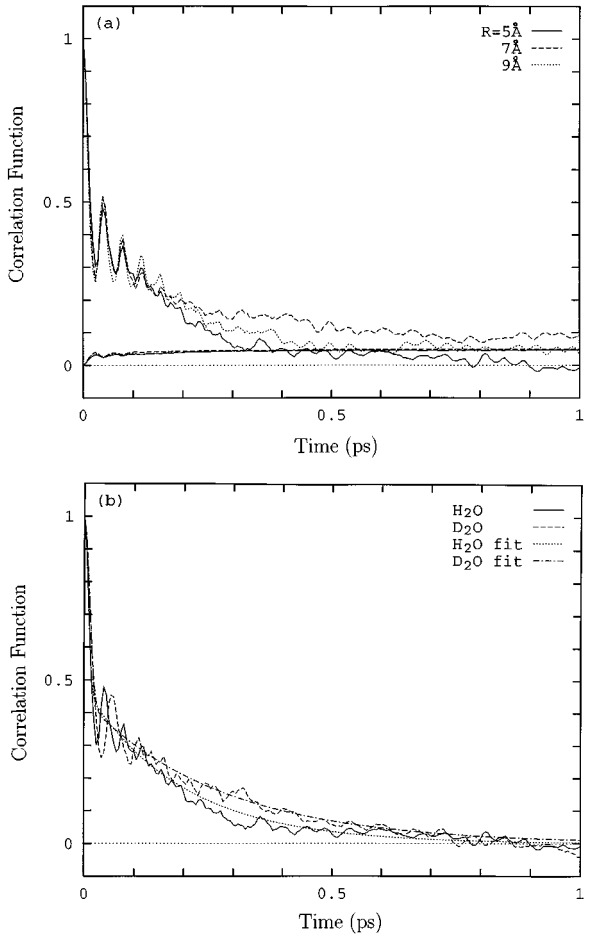

FIG. 3. (a) The time correlation function of the solvent coordinate Eq. (3.4) for H_2O solvent with the donor–acceptor distance $R=5$ (solid), 7 (dashed) and 9 (dotted) Å. The lower curves starting from the origin are the estimated simulation uncertainties (cf. Chap. 6 of Ref. 24). (b) Comparison between the time correlation functions for H_2O (solid) and D_2O (dashed) solvents. The donor–acceptor distance R is 5 Å. The least-squares fit curves of Eq. (3.5) are also included (dotted and dash-dotted curves). See Table II for the parameters.

$$A\,\exp(-t/\tau_1)+(1-A)\exp(-(t/\tau_2)^2). \tag{3.5}$$

The fit parameters and the half width at half maximum (HWHM) of the TCF are summarized in Table II.

TABLE II. Fit parameters of Eq. (3.5). R and τ are in Å and in fs, respectively.

	R	A	τ_1	τ_2	τ(HWHM)
	5	0.48	190	11	16
H_2O	7	0.47	260	9.9	15
	9	0.47	230	9.3	14
	5	0.44	270	15	20
D_2O	7	0.46	230	14	19
	9	0.46	290	13	18
	5	0.48	180	12	17
H_2O	7	0.46	230	12	17
(rigid)	9	0.46	150	10	14

C. Spectral density functions

The spectral density functions $J(\omega)$ of the solvent bath modes are computed from the cosine transform of the classical TCF,[38]

$$\langle \delta\Delta V(0)\,\delta\Delta V(t)\rangle_{\rm cl}=\frac{8}{\pi\beta}\int_0^\infty d\omega\,\frac{J(\omega)}{\omega}\cos\,\omega t, \tag{3.6}$$

in which β is the inverse temperature $\beta\equiv 1/k_BT$. Equation (3.6) is the classical limit ($\hbar\to 0$) of the symmetrized quantum TCF

$$\left\langle \tfrac{1}{2}[\,\delta\Delta V(0),\delta\Delta V(t)]_+\right\rangle$$

$$=\frac{4\hbar}{\pi}\int_0^\infty d\omega J(\omega)\coth\left(\frac{\beta\hbar\omega}{2}\right)\cos\,\omega t, \tag{3.7}$$

where $\Delta V(t)=e^{iH_it}\Delta V e^{-iH_it}$ and $[A,B]_+=AB+BA$. If we represent the Hamiltonian by a spin-boson form,[5]

$$H=|H_{\rm el}|\sigma_x-\frac{\Delta F^0}{2}\,\sigma_z+\sum_\alpha\left(\frac{p_\alpha^2}{2}+\frac{\omega_\alpha^2}{2}\,x_\alpha^2\right)$$

$$+\sigma_z\sum_\alpha\,c_\alpha x_\alpha, \tag{3.8}$$

where σ_x and σ_z are the usual Pauli spin matrices and $|H_{\rm el}|$ denotes the electronic coupling, then $J(\omega)$ is given by

$$J(\omega)=\frac{\pi}{2}\sum_\alpha\,\frac{c_\alpha^2}{\omega_\alpha}\,\delta(\omega-\omega_\alpha). \tag{3.9}$$

As is well known, the influence of the harmonic bath environment on the two-state ET system is solely described by $J(\omega)$. The correspondence between the quantum and classical densities of states via $J(\omega)$, as seen in Eqs. (3.6) and (3.7), is a key for the evaluation of the quantum rate constant summarized in the next subsection.

Because $J(\omega)$ relates to λ by the sum-rule

$$\lambda=\frac{4}{\pi}\int_0^\infty\frac{J(\omega)}{\omega}\,d\omega, \tag{3.10}$$

and because λ depends on R as seen in Sec. III A, the intensity of $J(\omega)$ is an increasing function of R. By normalizing $J(\omega)$ by an integral corresponding to λ,

$$\tilde{J}(\omega)\equiv J(\omega)\Big/\int_0^\infty\frac{J(\omega)}{\omega}\,d\omega, \tag{3.11}$$

we obtain results almost independent of R as displayed in Fig. 4.

The broadband up to $\sim$1000 cm^{-1} comes from the solvent translational, rotational and librational motions, which is essentially described by the rigid water models. Separate two bands near 1700 and 3700 cm^{-1} are due to intramolecular bending and stretching modes of water, respectively. The latter exhibits a splitting (presumably) coming from the symmetric and asymmetric stretchings.

Figure 4(b) shows that the dependence of $J(\omega)$ on the solute state (neutral or ion pair) is small, in parallel with the TCF results. This indicates that the dielectric saturation effect is negligible and supports the linear response assumption. This would be partly due to the large size and the zero or unit charge of the solute.[39] Figure 4(b) includes $\tilde{J}(\omega)$ for D_2O. The stretching band of D_2O also shows but smaller splitting. The peak frequencies for the three distinct bands are summarized in Table III. The isotope ratios are approximately $\sqrt{2}$ for all the bands. It was impossible to carry out the corresponding analysis for the lower-frequency components coming from the diffusive rotational and translational modes, which appear to determine the overall relaxation profile of the TCF.

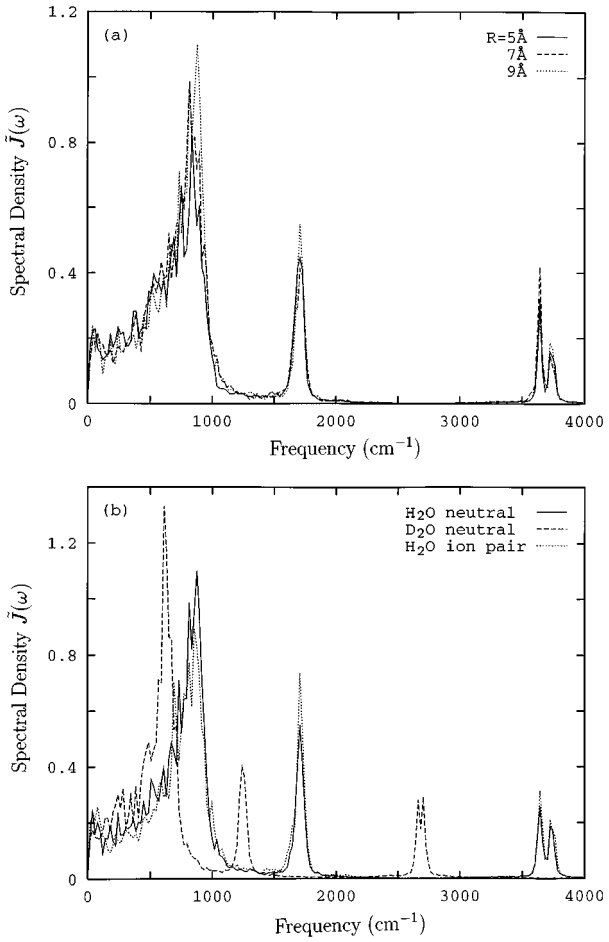

FIG. 4. (a). The normalized spectral density functions $\tilde{J}(\omega)$, corresponding to the time correlation functions of Fig. 3(a). (b) Comparison between $\tilde{J}(\omega)$ of H_2O (solid) and D_2O (dashed) in the neutral pair state of solute, and between $\tilde{J}(\omega)$ in the neutral (solid) and ion pair (dotted) states of the solute in H_2O solvent. The donor–acceptor distance R is 9 Å.

TABLE III. Peak frequencies of $J(\omega)$. ν is in cm^{-1}.

	H_2O	D_2O	$\nu_{(H_2O)}/\nu_{(D_2O)}$
ν(libration)	870	610	1.43
ν(bend)	1710	1240	1.38
ν(stretch-1)	3640	2670	1.36
ν(stretch-2)	3720	2710	1.37

TABLE IV. Decomposition of the reorganization energy. R and λ are in Å and in eV, respectively.

	R	λ (int.)	λ (bend)	λ (str.)
	5	1.765	0.060	0.015
H_2O	7	2.493	0.083	0.025
	9	3.060	0.103	0.027
	5	1.741	0.072	0.026
D_2O	7	2.490	0.084	0.026
	9	3.038	0.113	0.039

Now we discuss the microscopic details of the solvent reorganization energy on the basis of the computed $J(\omega)$. We decompose Eq. (3.10) into contributions from the three distinct bands of $J(\omega)$ by

$$\lambda(\text{int.})=\frac{4}{\pi}\int_0^{\omega_1}\frac{J(\omega)}{\omega}\,d\omega, \tag{3.12}$$

$$\lambda(\text{bend})=\frac{4}{\pi}\int_{\omega_1}^{\omega_2}\frac{J(\omega)}{\omega}\,d\omega, \tag{3.13}$$

$$\lambda(\text{str.})=\frac{4}{\pi}\int_{\omega_2}^{\omega_3}\frac{J(\omega)}{\omega}\,d\omega, \tag{3.14}$$

in which the low-frequency band is denoted as the ''intermolecular (int.)'' part. We used $\omega_{1,2,3}=1400$, 2500, 4000 cm^{-1} for H_2O and $\omega_{1,2,3}=1000$, 2000, 4000 cm^{-1} for D_2O, respectively. The computed results are shown in Table IV. The contributions from the solvent intramolecular vibrations are seen to be as small as 3%–4% (bend) and 1%–1.5% (str.). This provides a microscopic basis for the discussion in Sec. III A along with the results in Table I, where the reorganization energies of the flexible and rigid models are compared. This appears qualitatively (and intuitively) reasonable: The average bond lengths and angles of water do not differ much between the initial and final ET states, but the major portion of the solvent reorganization is covered by the reorientational polarization (and in addition, the translational density alteration). However, the solvent intramolecular modes do couple to ET dynamically, and exhibit marked quantum effects in the ET rate, as will be discussed in the following subsections.

We define the effective frequency Ω of the solvent coordinate by

$$\Omega^2\equiv\frac{\langle\delta\Delta\dot{V}^2\rangle_{\text{cl}}}{\langle\delta\Delta V^2\rangle_{\text{cl}}}, \tag{3.15}$$

where $\Delta\dot{V}$ denotes the time-derivative of ΔV. The simulation results are $\Omega=580\pm27$, 458 ± 24 and 430 ± 20 cm^{-1} for the flexible H_2O, D_2O and the rigid H_2O models, respectively (at $R=5$ Å in the neutral state). The results for different R ($=7$ and 9 Å) and for different solute states (neutral or ion pair) were approximately coincident within the simulation uncertainties. The effective frequency is also expressed in terms of the spectral density function by

$$\Omega^2=\frac{\int_0^\infty d\omega\ \omega J(\omega)}{\int_0^\infty d\omega\ J(\omega)/\omega}. \tag{3.16}$$

When $J(\omega)$ consists of separate multiple bands, as in the present case, it is not always adequate to represent the solvent coordinate dynamics by a single average frequency Ω. The elucidation of the distinctive roles played by fast and slow environmental modes is one of the recent central issues of ET mechanism.[40–42] This can be addressed on a microscopic basis by an analysis of the simulated $J(\omega)$, which will be reported elsewhere.

D. Quantum rate constants

The golden-rule rate formula of the ET rate

$$k_q=\frac{|H_{\text{el}}|^2}{\hbar^2}\int_{-\infty}^{+\infty}dt\langle e^{-iH_it/\hbar}e^{iH_ft/\hbar}\rangle_i, \tag{3.17}$$

is expressed in terms of $J(\omega)$ under the harmonic bath model by[5,14,15]

$$k_q=\frac{|H_{\text{el}}|^2}{\hbar^2}\int_{-\infty}^{+\infty}dt\ \exp[C_q(t)], \tag{3.18}$$

$$C_q(t)=\frac{i}{\hbar}\Delta F^0t+\frac{4}{\pi\hbar}\int_0^\infty d\omega\ \frac{J(\omega)}{\omega^2}\left\{(\cos\ \omega t-1)\coth\right.$$
$$\left.\times\left(\frac{\beta\hbar\omega}{2}\right)+i\ \sin\ \omega t\right\}. \tag{3.19}$$

The Condon approximation is invoked for the electronic coupling H_{el}. The oscillatory real-time integral of Eq. (3.19) is usefully evaluated by the method of steepest-descents

$$k_q\cong\frac{|H_{\text{el}}|^2}{\hbar^2}\sqrt{\frac{2\pi}{|C_q''(\tau^*)|}}\exp[C_q(\tau^*)], \tag{3.20}$$

in which the saddle-point of $C_q(t)$ is denoted by τ^* and C'' is the second time-derivative. Here, we define the ''quantum activation free energy'' [43] ΔF_q^* from the exponent of Eq. (3.20) by

$$-\beta\Delta F_q^*\equiv C_q(\tau^*). \tag{3.21}$$

The saddle-point is given by $\tau^*=i\beta\hbar/2$ for the symmetric ($\Delta F^0=0$) ET case. As we examine the energy gap dependence for the generic $J(\omega)$ from the simulation analysis, the saddle point was searched numerically on the imaginary-time axis by using the Newton-Raphson method.[28]

The absolute value of k_q depends strongly on R. Because H_{el} generally decreases exponentially by R and λ increases in proportion to $-1/R$, the absolute k_q and its dependence on ΔF^0 sharply vary as functions of R. But by defining $\Delta\widetilde{F}_q^*\equiv\Delta F_q^*/\lambda$ and $\Delta\widetilde{F}^0\equiv\Delta F^0/\lambda$, we obtain results almost independent of R as displayed in Fig. 5(a). The same renormalization of the R dependence into λ is immediately seen in the classical relation Eq. (1.1) as

$$\Delta\widetilde{F}_{\text{cl}}^*=(\Delta\widetilde{F}^0+1)^2/4. \tag{3.22}$$

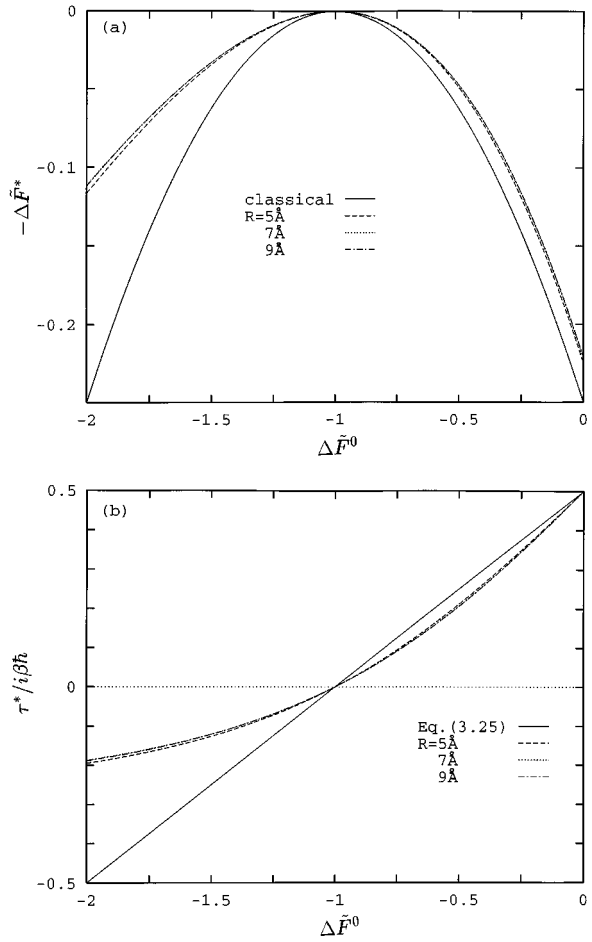

FIG. 5. (a) The renormalized quantum energy gap law, $\Delta\tilde{F}_q^* = \Delta F_q^*/\lambda$ plotted against $\Delta\tilde{F}^0 = \Delta F^0/\lambda$, for H_2O solvent with the donor–acceptor distance $R=5$ (dashed), 7 (dotted) and 9 (dash-dotted) Å. The classical $\Delta\tilde{F}_{\rm cl}^* = \Delta F_{\rm cl}^*/\lambda$ (solid) is included for comparison. (b) The imaginary-time saddle-point $\tau^*/i\beta\hbar$ as a function of the energy gap $\Delta\tilde{F}^0$. The curves correspond to those in Fig. 5(a). The approximation of Eq. (3.25) is also included (solid line).

The present results show that the scaling also applies for $\Delta\tilde{F}_q^*$ which essentially includes quantum effects such as the solvent nuclear tunneling. This is a consequence of the approximate R-independence of the normalized $\tilde{J}(\omega)$ of Eq. (3.11) as shown in Fig. 4(a).

The deviation of $\Delta\tilde{F}_q^*$ from the classical inverted parabola Eq. (3.22) comes from the quantum zero-point and tunneling effects of the solvent nuclear motions. The asymmetry of ΔF_q^* about $\Delta F^0=-\lambda$ axis is due to the larger tunneling effect in the inverted region because of the smaller width of the potential barrier than in the normal region. This asymmetry is not accounted for by the ''semiclassical'' and an equivalent ''short-time'' approximations (see Sec. III F). The qualitative points of these have been discussed previously for simple models.[11] We rather stress the marked quantum effects at the room temperature found for the realistic water model. The large contribution of the solvent intramolecular modes despite their small reorganization energy is noteworthy, as described in the next subsection.

Now we discuss some details of the saddle-point calculation. First we briefly summarize the idea following Ref. 17, and then show a connection between the saddle-point and the energetic quantities with the numerical results. The argument here is not restricted to the harmonic bath model, and we directly invoke the steepest-decents method to Eq. (3.17). The exponential part of Eq. (3.20), that has an imaginary TCF form, is read as a ratio of two thermodynamic partition functions

$$\exp[C(\tau^*)] = \frac{\mathrm{Tr}\{e^{-(\beta-\beta^*)H_i}e^{-\beta^* H_f}\}}{\mathrm{Tr}\{e^{-\beta H_i}\}}, \tag{3.23}$$

in which we defined $i\beta^*\hbar \equiv \tau^*$. The path integral representation[44] of the numerator is written as an integral over paths on the two diabatic potential surfaces V_i and V_f,

$$\int D\mathbf{x}(\tau)\exp\Big\{-\frac{1}{\hbar}\int_0^{\beta\hbar} d\tau \sum_\alpha \frac{m_\alpha}{2}\dot{x}_\alpha^2 + \theta(\beta^*\hbar-\tau)V_i[\mathbf{x}(\tau)] + \theta(-\beta^*\hbar+\tau)V_f[\mathbf{x}(\tau)]\Big\}. \tag{3.24}$$

The denominator is expressed similarly but without the step functions. By discretizing the path integral,[45] partition functions of interacting ''polymers'' distributing around the diabatic surface crossing are obtained. As Eq. (3.24) implies, the argument applies in the region $-\lambda<\Delta F^0<\lambda$.

The saddle-point β^* corresponds to the number ratio between the polymer ''beads'' on the different potential surfaces. From this we inspect that β^* may be correlated to the ratio between the *slopes* of the two free energy curves (denoted by F_i' and F_j') at the curve crossing,

$$\frac{\beta^*}{\beta} \simeq \frac{|F_i'|}{|F_i'|+|F_f'|} = \frac{1}{2}\left(1+\frac{\Delta F^0}{\lambda}\right). \tag{3.25}$$

Figure 5(b) plots τ^* as a function of $\Delta\tilde{F}^0$ for the present system. The solid line displaying Eq. (3.25) is seen to be a good approximation in its applicable (i.e., the normal) region. In the inverted region, the decrease of τ^* slows down to deviate from Eq. (3.25). Indeed, the right-hand-side of Eq. (3.25) is known as an approximate saddle-point for harmonic cases.[2,11] The alternative view of the connection to the slopes at the curve crossing exploited here[22] seems versatile to apply for other cases such as anharmonic systems, which will be pursued elsewhere.

Figure 6 displays the isotope dependence of the energy gap law. The renormalized activation free energy difference, $\delta\Delta\tilde{F}^* \equiv \Delta\tilde{F}^*_{(D_2O)} - \Delta\tilde{F}^*_{(H_2O)}$, was 1.5×10^{-2}, 1.4×10^{-6} and 5.2×10^{-3} at $\Delta\tilde{F}^0=-2$, -1 and 0, respectively for $R=5$ Å. Values of the same order were obtained for $R=7$ and 9 Å. Thus the actual difference of the activation free energy is adequately scaled by λ.

E. Comparison with rigid water model

The main results of the present paper are for the flexible water model. Here, we compare them with the rigid water model in order to quantify the role of the solvent intramolecular vibrational modes. Figure 7(a) shows the comparison

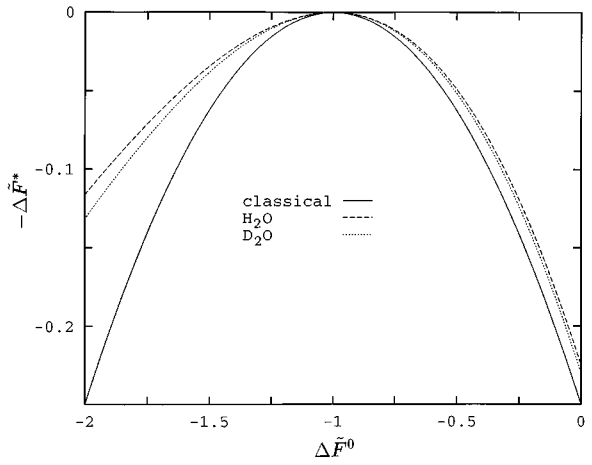

FIG. 6. Comparison between the quantum activation free energies $\Delta\tilde{F}_q^* = \Delta F_q^*/\lambda$ for H_2O (dashed) and D_2O (dotted) solvents. The classical curve (solid) is included for reference. The donor–acceptor distance R is 5 Å.

of $J(\omega)$. The rigid model has no bending and stretching bands. The low-frequency band is quite similar between the two models, which is also reflected in the similarity of the TCF. It is noted, however, that the tail of the libration band around 1000 cm^{-1} extends longer for the flexible model. This is seen for all R's examined (5, 7 and 9 Å), though only the result for $R=7$ Å is shown.

The comparison of $\Delta\tilde{F}_q^*$ is displayed in Fig. 7(b). The enhancement of the tunneling effect due to the solvent intramolecular vibrations is remarkable especially in the inverted region, i.e., where the quantum effects are larger. In addition, we computed $\Delta\tilde{F}_q^*$ by truncating $J(\omega)$ of the flexible model at 1300 cm^{-1} to remove the intramolecular bands. As seen in Fig. 7(b), this gives the result close to that for the rigid model, but showing slightly larger tunneling presumably due to the longer tail of the librational band mentioned above.

To summarize, the intramolecular vibrations of the solvent water emerge as the prominent factor for the quantum aspects of ET, despite that their contributions in the static reorganization energy are quantitatively small. Nonetheless, it is seen that the low-frequency component (and the rigid model) itself shows notable quantum effects. Thus care should be paid on representing the solvent reorientational polarization by a ''slow'' classical mode, as occasionally employed in experimental analyses, for aqueous ET reactions.

The flexible and rigid models give quite similar TCF curves. The high-frequency components on the TCF seen only for the flexible model are very weak. The fit parameters to Eq. (3.5) are compared in Table II, showing small difference between the two models.

F. Simulating quantum rates

Here, we briefly reexamine the ET rate formula in light of the present simulation results. The cumulant expansion of Eq. (3.17) to second-order (after rewriting it into a time-ordered exponential form) gives[14,15]

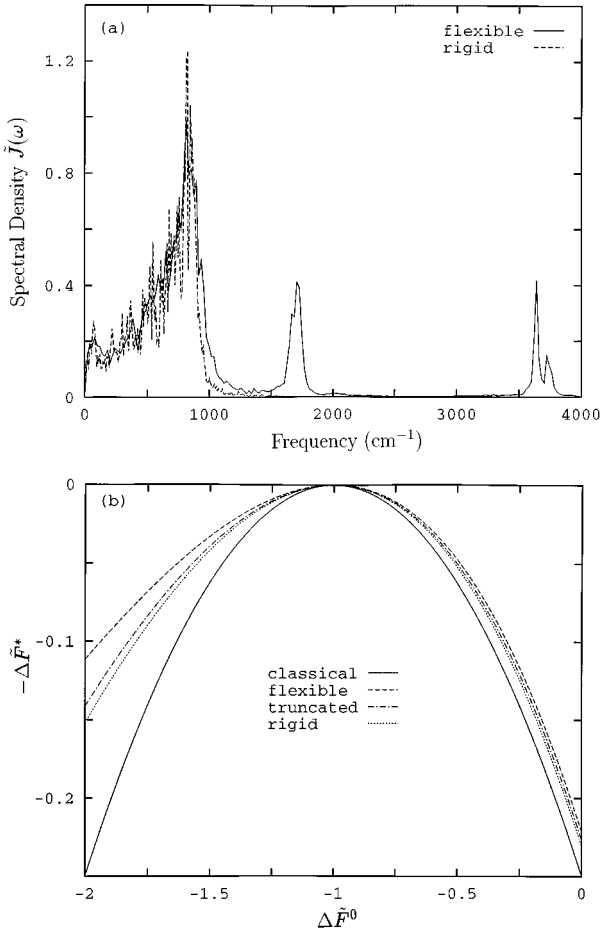

FIG. 7. (a) Comparison between the spectral density functions $\tilde{J}(\omega)$ of the flexible (solid) and rigid (dashed) models of H_2O. The donor-acceptor distance R is 7 Å. (b) Comparison between the quantum activation free energies $\Delta\tilde{F}_q^* = \Delta F_q^*/\lambda$ of the flexible (dashed) and rigid (dotted) H_2O models. The result from the truncated $J(\omega)$ of the flexible model (dash-dotted) is also included (see the text). The solid curve is the classical reference. The donor–acceptor distance R is 7 Å.

$$k_q = \frac{|H_{\rm el}|^2}{\hbar^2}\int_{-\infty}^{+\infty} dt\ \exp\left[-\frac{i}{\hbar}\langle\Delta V\rangle_i t + \left(\frac{i}{\hbar}\right)^2\int_0^t d\tau(t-\tau)\times\langle\delta\Delta V(0)\,\delta\Delta V(\tau)\rangle_i\right]. \tag{3.26}$$

Here, we introduce two approximations. The second one is well known and has been discussed repeatedly, while the first one would not be. The first one replaces the TCF in Eq. (3.26) by the symmetrized Eq. (3.7) to give

$$k_{q+} = \frac{|H_{\rm el}|^2}{\hbar^2}\int_{-\infty}^{+\infty} dt\ \exp[C_{q+}(t)], \tag{3.27}$$

$$C_{q+}(t) = \frac{i}{\hbar}(\lambda+\Delta F^0)t + \frac{4}{\pi\hbar}\int_0^\infty d\omega\ \frac{J(\omega)}{\omega^2}\times[\cos\omega t - 1]\coth\left(\frac{\beta\hbar\omega}{2}\right). \tag{3.28}$$

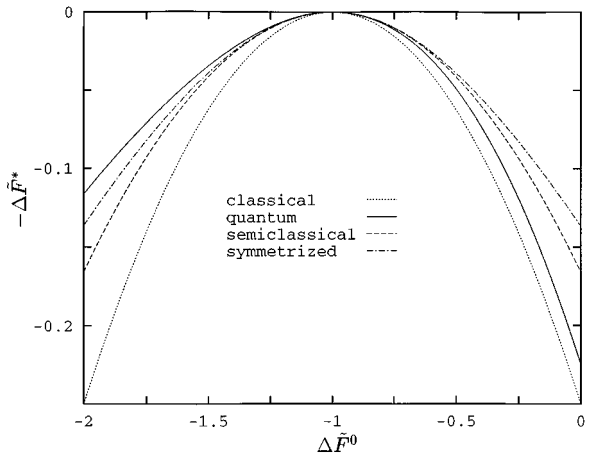

FIG. 8. The quantum energy gap law for various approximation formulae; quantum (solid), semiclassical (dashed), symmetrized (dash-dotted), and classical (dotted). See Sec. III F for details.

The second approximation is most straightforwardly obtained by expanding either C_q or C_{q+} in powers of t and truncating at the second-order (''short-time approximation'') to give

$$k_{\rm st}=\frac{|H_{\rm el}|^2}{\hbar}\sqrt{\frac{\pi\beta}{\Lambda}}\exp\left\{-\beta\frac{(\lambda+\Delta F^0)^2}{4\Lambda}\right\}, \tag{3.29}$$

$$\Lambda=\frac{2\beta\hbar}{\pi}\int_0^\infty d\omega\, J(\omega)\coth\left(\frac{\beta\hbar\omega}{2}\right). \tag{3.30}$$

This is equivalent to the so-called ''semiclassical'' approximation which neglects the commutator $[H_i,H_f]$. Λ may be termed the ''quantum-corrected reorganization energy'' [46] as it goes to the classical λ in the limit of $\beta\hbar\to 0$. All of k_q, k_{q+} and $k_{\rm st}$ reduce to the well known form that includes λ instead of Λ in Eq. (3.29) in the classical limit.

Figure 8 compares the quantum activation free energies corresponding to k_q, k_{q+} and $k_{\rm st}$. Large deviations of $\Delta\tilde{F}^*_{q+}$ and $\Delta\tilde{F}^*_{\rm st}$ from $\Delta\tilde{F}^*_q$ are notable not only quantitatively but also qualitatively: The required asymmetry of the energy gap law about $\Delta F^0=-\lambda$ is not correctly described in $\Delta\tilde{F}^*_{q+}$ and $\Delta\tilde{F}^*_{\rm st}$. The symmetric behavior of these two is immediately seen in the forms Eqs. (3.28) and (3.29). Especially, the former is usefully compared below with the asymmetric form of Eq. (3.19). The latter was discussed by Siders and Marcus[11] to be the consequence of the replacement of the δ-function of energy by that of the potential energy in the golden-rule rate formula. Bader *et al.* argued the special ($\Delta F^0=0$) case of Eq. (3.29) in terms of the centroid path density of the quantum transition state theory.[7] Here, we deal with k_{q+} rather than $k_{\rm st}$ in terms of the TCF formalism. It is seen by comparing Eqs. (3.19) and (3.28) that the qualitatively required asymmetry of the quantum energy gap law is represented by

$$C_{q+}(t)-C_q(t)=\frac{i}{\hbar}\left\{\lambda t-\frac{4}{\pi}\int_0^\infty d\omega\,\frac{J(\omega)}{\omega^2}\sin\omega t\right\}. \tag{3.31}$$

Thus the term coming from the imaginary-part of the quantum TCF is seen to be essential for an adequate description of the solvent nuclear quantum aspects. Similar argument would apply for evaluation of other quantum rates and spectral properties with the use of the MD trajectory data.[47] Equation (3.31) vanishes in the limit of $\omega t\to 0$. With some characteristic frequency $\overline{\omega}$ (which may be Ω in Sec. III C), and the approximate τ^* of Eq. (3.25), the condition for Eq. (3.31) being small is expressed by $\beta\hbar\overline{\omega}(1+\Delta\tilde{F}^0)\simeq 0$, i.e., $\Delta F^0\simeq-\lambda$ in addition to the usual high-temperature and low-frequency conditions.

IV. CONCLUDING REMARKS

The rate formula Eqs. (3.17)–(3.19) employed in this work represents the perturbation expansion of the second-order in $H_{\rm el}$ (the first-order process). This essentially includes the solvent dynamical effects in a sense that it explicitly includes the spectral density function obtained from the realistic MD simulation. A possible extension of this work would compute the fourth and higher order terms of $H_{\rm el}$. Although they are formally known for the two-state harmonic bath model, the actual computation of the multiple integrals with an input of the simulated spectral density functions is not straightforward. The noninteracting-blip approximation[5] by Leggett *et al.* provides a way to evaluate the perturbation series of all-order, though it might not be appropriate for investigation of the energy gap dependence.[5] It would be also possible to compute the fourth-order term and derive a renormalized rate formula[48] with the use of the second and fourth-order terms.

Another extension would relax the thermal equilibrium assumption. This would include two aspects; (i) the competition between the electronic transition and the solvent relaxation processes, and (ii) the division of the environmental motions into fast and slow (nonequilibrium) components. Both represent the recent central issues of the theory of electronic transitions in condensed phases.[40,49,50] A microscopic analysis of these based on the simulated spectral density functions such as the present one would enrich our realistic understanding. Works along these lines will be reported in subsequent publications.

It would be also of interest to compare the present results with more elaborate PIQMC calculations. To our knowledge, the latter has not been performed for flexible water models. As the PIQMC directly evaluates Eq. (3.23),[7] the two approaches would give equivalent results (at any temperature) for precisely harmonic systems, apart from the differences in the numerical approximations. The anharmonicity may become more significant than the present cases for shorter distance ETs such as intramolecular charge transfers. We note, however, that the solvent nuclear quantum effects are expected to be smaller for the short-range ETs since they are appropriately scaled by the solvent reorganization energy as shown in Sec. III D.

The present work has demonstrated the importance of the high-frequency intramolecular modes of the solvent water that involve the light hydrogen vibrations. Most part of

the considerations here on ET would also apply for other quantum processes in water such as electron hydration,[51] proton transport[52] and acid-base reactions.[53,54] The quantum aspects of the solvent vibrational coupling in these more complicated processes are yet unclear. Other protic solvents like alcohols may also show marked quantum effects involving the stretching and bending motions of the OH part. The same would apply for cases where the OH part of the protein side-chains and/or the excess waters in the active-site region couple to enzymatic reactions. Theoretical/computational works on some of these issues are now under way and will be reported in the future.

ACKNOWLEDGMENTS

This work was initiated with a support by Special Postdoctoral Researchers Program at RIKEN and was completed at the University of Tsukuba. Large-scale simulations were carried out on Fujitsu VPP500 at RIKEN Supercomputer Center. The author is grateful to Dr. A. Kira and the members of Chemical Dynamics Lab at RIKEN for their encouragements. He also thanks Professor H. Sumi for his interest and useful comments.

[1] H. Beens and A. Weller, in *Organic Molecular Photophysics*, edited by J. B. Birks (Wiley Interscience, London, 1975); *Dynamics and Mechanisms of Photoinduced Electron Transfer and Related Phenomena*, edited by N. Mataga, T. Okada, and H. Masuhara (Elsevier, Amsterdam, 1992); *Electron and Proton Transfer Processes in Chemistry and Biology*, edited by A. Müller, H. Ratajczak, W. Junge, and E. Diemann (Elsevier, Amsterdam, 1992).
[2] J. Ulstrup, *Charge Transfer Processes in Condensed Media* (Springer, Berlin, 1979).
[3] M. D. Newton and N. Sutin, Annu. Rev. Phys. Chem. **35**, 437 (1984); R. A. Marcus and N. Sutin, Biochim. Biophys. Acta. **811**, 265 (1985).
[4] R. A. Marcus, J. Chem. Phys. **24**, 966, 979 (1956); Ann. Rev. Phys. Chem. **15**, 155 (1964).
[5] For example, A. J. Leggett, S. Chakravarty, A. Dorsey, M. P. A. Fisher, A. Garg, and W. Zwerger, Rev. Mod. Phys. **59**, 1 (1987) and references therein.
[6] J. K. Hwang and A. Warshel, J. Am. Chem. Soc. **109**, 715 (1987); A. Warshel and J. K. Hwang, J. Chem. Phys. **84**, 4938 (1986); A. Warshel, Z. T. Chu, and W. W. Parson, Science **246**, 112 (1989).
[7] J. S. Bader, R. A. Kuharski, and D. Chandler, J. Chem. Phys. **93**, 230 (1990).
[8] C. L. Kneifel, M. D. Newton, and H. L. Friedman, J. Mol. Liq. **60**, 107 (1994).
[9] D. Rehm and A. Weller, Isr. J. Chem. **8**, 259 (1970); A. Kira, J. Phys. Chem. **85**, 3047 (1981); G. L. Closs, L. T. Calcaterra, N. J. Green, K. W. Penfield, and J. R. Miller, *ibid*. **90**, 3673 (1986).
[10] M. Tachiya, J. Phys. Chem. **93**, 7050 (1989); A. Yoshimori, T. Kakitani, Y. Enomoto, N. Mataga, *ibid*. **93**, 8316 (1989); J. Tang, J. Chem. Phys. **99**, 5828 (1993).
[11] P. Siders and R. A. Marcus, J. Am. Chem. Soc. **103**, 741, 748 (1981).
[12] R. A. Marcus and P. Siders, J. Phys. Chem. **86**, 622 (1982).
[13] It is noted that the high-temperature formula for harmonic systems does not include entropy terms coming from frequency changes. Equation (1.1) is more general in this respect.
[14] R. Kubo and Y. Toyozawa, Prog. Theor. Phys. **13**, 160 (1955).
[15] M. Lax, J. Chem. Phys. **20**, 1752 (1952).
[16] J. J. Hopfield, Proc. Natl. Acad. Sci. USA **71**, 3640 (1974).
[17] P. G. Wolynes, J. Chem. Phys. **87**, 6559 (1987).
[18] C. Zheng, J. A. McCammon, and P. G. Wolynes, Proc. Natl. Acad. Sci. USA **86**, 6441 (1989); C. H. Mak and J. N. Gehlen, Chem. Phys. Lett. **206**, 130 (1993); R. Egger and C. H. Mak, J. Chem. Phys. **99**, 2541 (1993).
[19] M. Maroncelli and G. R. Fleming, J. Chem. Phys. **89**, 5044 (1988).
[20] K. Ando and S. Kato, J. Chem. Phys. **95**, 5966 (1991).
[21] M. Cho, G. R. Fleming, S. Saito, I. Ohmine, and R. M. Stratt, J. Chem. Phys. **100**, 6672 (1994).
[22] K. Ando, J. Chem. Phys. **101**, 2850 (1994).
[23] M. D. Newton, Int. J. Quantum Chem. S **14**, 363 (1980); Y.-P. Liu and M. D. Newton, J. Phys. Chem. **99**, 12382 (1995); G. Karlström P.-A. Malmqvist J. Chem. Phys. **96**, 6115 (1992).
[24] For example, M. P. Allen and D. J. Tidesley, *Computer Simulation of Liquids* (Clarendon, Oxford, 1987).
[25] W. L. Jorgensen, J. Chandrasekhar, J. Madura, R. W. Impey, and M. L. Klein, J. Chem. Phys. **79**, 926 (1983).
[26] L. X. Dang and B. M. Pettitt, J. Phys. Chem. **91**, 3349 (1987).
[27] C. W. Gear, *Numerical Initial Value Problems in Ordinary Differential Equations* (Prentice-Hall, Englewood Cliffs, 1971).
[28] For example, W. L. Press, B. P. Flannery, S. A. Teukolsky, and W. T. Vetterling, *Numerical Recipes: The Art of Scientific Computing* (Cambridge University Press, New York, 1989).
[29] W. F. van Gunsteren and H. J. C. Berendsen, Mol. Phys. **34**, 1311 (1977).
[30] Several 10 ps of cooling and 20 ps of equilibration runs were first carried out for the rigid water system. Then the intramolecular vibration of the solvent was turned on. The atom velocities were scaled to 298 K at every 5000 steps (=0.5 ps) which was repeated ten times (and practically more associated with the program development). After this cooling/heating procedure, an equilibration run was performed for more than 20 ps by using the constant temperature method by Berendsen *et al.* (Ref. 31) to keep the kinetic temperature around 298 K. The relaxation time parameter of the method was set to be 0.4 ps. In these cooling and equilibration runs, the r-RESPA method (Ref. 32) was employed for the flexible water model in order to save the computational cost. The long-range forces from outside the primary region (in a sphere of 6 Å radius containing 39 molecules in average) of each molecule were updated every 5 (for cooling) or 10 (for equilibration) microsteps with $\Delta t_{\mathrm{micro}}=0.1$ fs. The r-RESPA method was used *only* for the cooling and equilibration runs and *not* for the production runs reported in text.
[31] H. J. C. Berendsen, J. P. M. Postma, W. F. van Gunsteren, A. Di Nola, and J. R. Haak, J. Chem. Phys. **81**, 3684 (1984).
[32] M. Tuckerman, B. J. Berne, and G. J. Martyna, J. Chem. Phys. **97**, 1990 (1992).
[33] The usefulness of the ΔV coordinate is also seen in its connection to the Franck–Condon surface hopping picture, as the two diabatic potentials always coincide at $\Delta V=0$. See also the golden-rule rate formula of Eq. (3.17).
[34] The simulation uncertainties were evaluated with the use of the correlation time computed from the TCF of Sec. III B. See Chapter 6 of Ref. 24.
[35] M. Tachiya and S. Murata, J. Phys. Chem. **96**, 8441 (1992); M. Tachiya and M. Hilczer, in *Ultrafast Reaction Dynamics and Solvent Effects: Theoretical and Experimental Aspects*, edited by Y. Gauduel and P. J. Rossky (AIP, New York, 1994).
[36] It is possible to generalize Eq. (3.3) to take account of the cavity overlap: B. J. Gertner, K. Ando, R. Bianco, J. T. Hynes, Chem. Phys. **183**, 309 (1994).
[37] For discussions on different polar solvents (acetonitrile and methyl chloride), M. Maroncelli, J. Chem. Phys. **94**, 2034 (1991); E. A. Carter and J. T. Hynes, *ibid*. **94**, 5961 (1991).
[38] The cosine transform of the TCF is computed from the power-spectrum of the ΔV trajectory (Wiener-Khinchin theorem), by using the FFT (fast Fourier transform) method. The Bartlett window was applied to reduce the finite truncation bias (Ref. 28). The 5×10^5 steps (=50 ps) data was divided into and averaged over 30 parts with the length of 2^{14} steps. This length gives the frequency resolution of 20.3 cm^{-1}.
[39] Our $J(\omega)/\omega$ corresponds (apart from a constant factor) to $I(\omega)$ in Ref. 8 for ferros-ferric exchange ET in a flexible water model. They also computed the spectra of the hydrogen atom velocity-auto-correlation functions, which shows a broad stretching band coming from the strong coordination of the ligand water to the small ions. Its peak position notably shifts depending on the ion charge.
[40] L. D. Zusman, Chem. Phys. **49**, 295 (1980); *ibid*. **80**, 29 (1983); H. Sumi and R. A. Marcus, J. Chem. Phys. **84**, 4894 (1985); A. Garg, J. N. Onuchic, and V. Ambegaokar, *ibid*. **83**, 4491 (1985); J. Jortner and M. Bixon, *ibid*. **88**, 167 (1988); T. Fonseca, *ibid*. **91**, 2869 (1989).
[41] B. B. Smith, A. Staib, and J. T. Hynes, Chem. Phys. **176**, 521 (1993).
[42] G. C. Walker, E. Åkesson, A. E. Johnson, N. E. Levinger, and P. F. Barbara, J. Phys. Chem. **96**, 3728 (1992); K. Tominaga, D. A. V. Kliner,

A. E. Johnson, N. E. Levinger, and P. F. Barbara, J. Chem. Phys. **98**, 1228 (1993).

[43] Here the term ''free energy'' is rather loosely used. The entropy change ΔS^0 is zero for the harmonic bath model leading Eqs. (3.17)–(3.19). As seen by comparing $J(\omega)$ of the initial and final states in Fig. 4(b), this is a reasonable approximation for the present system. If the inner-sphere vibrations of the solute species were taken into account, ΔS^0 may become important, which could be adequately modeled by employing averaged force constants.

[44] R. P. Feynman and A. R. Hibbs, *Quantum Mechanics and Path Integrals* (McGraw-Hill, New York, 1965).

[45] D. Chandler and P. G. Wolynes, J. Chem. Phys. **74**, 4078 (1981).

[46] In other words, Λ is related to a ''quantum-corrected variance of distribution'' of the solvent coordinate (Ref. 16).

[47] J. S. Bader and B. J. Berne, J. Chem. Phys. **100**, 8359 (1994).

[48] H. Sumi, J. Phys. Soc. Jpn. **49**, 1701 (1980); M. Sparpaglione and S. Mukamel, J. Chem. Phys. **88**, 3263 (1988).

[49] N. Shima and M. Tsukada, Surf. Sci. **194**, 3121 (1988); M. Tsukada and Z. W. Gortel, Phys. Rev. B **38**, 3892 (1988).

[50] J. N. Onuchic and P. G. Wolynes, J. Phys. Chem. **92**, 6495 (1988); J. M. Jean, R. A. Friesner, and G. R. Fleming, J. Chem. Phys. **96**, 5827 (1992); R. D. Coalson, D. G. Evans, and A. Nitzan, *ibid*. **101**, 436 (1994).

[51] For recent works, see, for example, P. J. Rossky and J. D. Simon, Nature (London) **370**, 263 (1994); E. Neria and A. Nitzan, J. Chem. Phys. **99**, 1109 (1993); Y. Kimura, J. C. Alfano, P. K. Walhout, and P. F. Barbara, J. Phys. Chem. **98**, 3450 (1994).

[52] For example, G. W. Robinson, P. J. Thistlethwaite, and J. Lee, J. Phys. Chem. **90**, 4224 (1986); A. S. Davydov, *Solitons in Molecular Systems* (Naukovaja Dumka, Kiev, 1984); T. Komatsuzaki and I. Ohmine, Chem. Phys. **180**, 239 (1994); Mol. Sim. **16**, 321 (1996); M. Tuckerman, K. Laasonen, M. Sprik, and M. Parrinello, J. Phys. Chem. **99**, 5749 (1995); J. Chem. Phys. **103**, 150 (1995).

[53] K. Ando and J. T. Hynes, J. Mol. Liq. **64**, 25 (1995); Discuss. Faraday Soc. (in press).

[54] For example, W. P. Jencks, *Catalysis in Chemistry and Enzymology* (McGraw-Hill, New York, 1969); M. Eigen, W. Kruse, and L. De Maeyer, Prog. React. Kin. **2**, 285 (1964); W. J. Albery, *ibid*. **4**, 353 (1967); K. Laasonen and M. L. Klein, J. Am. Chem. Soc. **116**, 11620 (1994).